Port Reduction Operation of a Three-port Nonagonal Modular Multilevel Converter as Soft Open Point

Wenjun Liu[1,2] | Jiahao Yan[1,2] | Zhiwen Qin[1,2] | Bo Yuan[3] | Yaoqiang Wang[1,2] | Jun Liang[4]

[1]School of Electrical and Information Engineering, Zhengzhou University, Zhengzhou, China
[2]Henan Engineering Research Center of Power Electronics and Energy Systems, Zhengzhou, China
[3]China Aviation Optical-Electrical Technology Co. Luoyang City, China
[4]School of Engineering, Cardiff University, Cardiff, U.K.

Correspondence
Yaoqiang Wang, School of Electrical and Information Engineering, Zhengzhou University,
Email: WangyqEE@163.com

Funding information
Project supported by the National Natural Science Foundation of China (52007171)

Abstract

Nonagonal modular multilevel converter (MMC) is a three-port AC-AC converter promising as a soft open point (SOP) to connect different AC feeders or buses in distribution networks, owing to its flexible power control, transformerless structure, low power component count and its capable of accommodating multiple AC ports of different frequencies. An SOP should be able to work under port reduction condition which is often encountered when maintenance is required or the network structure is reconfigured. However, as a component reuse converter of circular structure, nonagonal MMC cannot turn off one or some of its branches to achieve this. To address this issue, a control scheme is proposed in this paper to enable nonagonal MMC to operate under port reduction condition by switching the nonagonal MMC to a hexagonal MMC which is an AC-AC topology of a similar circular structure but has only two ports. Without inserting extra switches, the nine branches of nonagonal MMC is redistributed into six branches. By alternately operating the submodules, no submodules need to be shut down, reducing the submodule capacitor voltage fluctuation during port reduction operation. RTlab results verify the feasibility of the quasi-hexagonal topology and the effectiveness of port reduction control.

KEYWORDS

Distributed power generation, multilevel converters, multiport converter, control strategy

1 | INTRODUCTION

The discontinuity nature of renewable energy sources and its increasing penetration in power grid is a great challenge for the stable operation of distributed networks. [1,2,3] Further complicated by power loads such as electric vehicles, the distribution network is likely to suffer from unbalanced voltages, uneven power distribution, higher peak and fault currents. To ensure the stability, power quality and efficiency of the network, soft open points (SOPs) are implemented. [4] Power converters with high efficiency and modularity are explored as possible SOP topologies with a power level fit for distribution networks. [5,6]

To achieve the aforementioned aims, many power conversion topologies have been proposed in the literature. As a relatively mature high-power topology, the cascaded H-bridge multilevel converter is made up by cascaded H-bridge submodules each with an AC/DC front-end connected with isolated low-voltage inputs. [7,8] However, it requires a multi-winding transformer to obtain the multiple isolated low-voltage inputs needed, which greatly increases the cost and power loss. [9,10] Compared with cascaded multilevel converters, modular multilevel converters (MMC) do not require multiple isolated low-voltage ports as inputs, hence eliminating the need for multi-winding transformers. [11] Modularity, scalability, low power losses, and low harmonic distortion are some of the notable features that recommend MMC for high-power applications (static synchronous compensators, medium-voltage motor drives etc.). [12,13] Furthermore, MMC can be configured to perform AC/AC conversion and connect different AC feeders or buses of a distributed network. [4] Two MMCs can form an indirect AC/AC converter by sharing a high-voltage DC link, which is named as back-to-back MMC. Back-to-back MMC can both avoid the transformer and accommodate higher voltage due to its modular design, but the high-voltage DC link would reduce the low frequency performance. [14,15] Besides, the application of back-to-back MMC on distribution networks is very restricted by cost, footprint, reliability and power losses. In comparison, direct AC/AC converter is an attractive alternative to the back-to-back converter. [16]

Modular multilevel matrix converter (M3C) is a typical direct AC/AC converter. It is made up by nine branches connected in 3 ×3 configuration, each branch consisting of multiple H-bridge submodules cascaded together. [17] In [18], M3C is used in FFTS and a zero-sequence current mitigation controller for M3C is implemented and tested. In addition, M3C have high redundancy and can maintain operation of both AC ports in the condition of branch failure. [19] In comparison with M3C, hexagonal MMC can achieve direct AC/AC conversion using only six branches instead of nine, which greatly reduces equipment volume and production cost. [20] It is attractive as an SOP connecting two three-phase systems due to its simplicity. [16] In [19], the hexagonal MMC is considered as an alternative of M3C under branch failure, and the transition from M3C to hexagonal MMC is discussed in [21]. In [22], a

branch voltage balancing control is proposed that uses zero sequence voltage and hex-loop circulating current to ensure DC voltage stability. In [23], a circulating current suppression control is proposed for it to attenuate the circulating current flowing in the branches and reduce submodule capacitor voltage fluctuation. A nonagonal MMC is proposed in [24], [25] based on the dual-port hexagonal MMC. By adding three branches in the loop structure, the nonagonal MMC is able to accommodate three AC ports. It retains hexagonal MMC's superiorities in size and low frequency performance, while further enhances its advantage in power component count. The nonagonal MMC is a competitive SOP topology. [26] However, the research on this topology is still in the initial state. Current literatures studying nonagonal MMC focuses mostly on attenuating the current stress [26] and submodule capacitor fluctuation [27] to further enhance its advantage in cost, but has not discussed extensively the problems it would encounter when used in industrial application.

As an SOP topology, the converter should be able to operate under port reduction condition in case of network reconfiguration. [4] For an SOP without component reuse, it can be achieved by turning off the branches corresponding to the offline port. [28] However, nonagonal MMC faces three challenges:

1) Component reuse: [29] Nonagonal MMC is a component reuse topology, all nine branches participate in the energy transfer of any two ports.

2) Loop structure: Nonagonal MMC is of loop structure. By shutting down one branch, the loop structure will be injured and the energy transfer path will be blocked.

3) Power balance: Nonagonal MMC needs to inject offset voltages to ensure the overall power balance. When one port is turned off, the power balance condition changes.

Due to the first two challenges, the nonagonal MMC cannot work under dual port condition by simply shutting down the branches connected to the offline port. [28] Due to the third challenge, power balance control has to be adjusted to ensure its stable operation during port reduction operation.

To address this issue, this paper proposes a port reduction control which enables the nonagonal MMC to turn off the offline port and operate under a dual port condition during port reduction. The main idea of the port reduction control is to switch the nine-branch nonagonal MMC to a six-branch hexagonal MMC. Instead of bypassing the surplus branches and leaving their submodule capacitors floating, branches connected with the same phase of the offline port are combined. Hence, the nine branches of nonagonal MMC are redistributed into six branches, and the submodules are turned on alternately so that the submodule capacitor voltages are still controllable during port reduction operation.

The paper is organized as follows. The nonagonal MMC topology and its power analysis are presented in Section II. In Section III, the port reduction topology is derived, and the operation principle is analyzed. Based on this, in Section IV, a port reduction operation control method is proposed for the nonagonal MMC to allow the nonagonal MMC to continue to operate under a dual port condition, and its performance is verified on RTLAB simulation platform in Section V. Finally, Section VI summarizes this study.

2 | THREE-PORT NONAGONAL MMC TOPOLOGY AND POWER ANALYSIS

2.1 | Nonagonal MMC topology

The structure of the three-port nonagonal MMC is shown in Fig. 1. Nonagonal MMC consists of nine identical branches forming a nonagonal ring. Each branch has n identical H-bridge submodules with an AC inductor connected in series. The input/output ports are introduced from the connection points of its nine branches. The three phases of the three ports are depicted as: x, y, z for Port 1, r, s, t for Port 2, and u, v, w for Port 3. According to which phase they are connected with, the nine vertexes of nonagonal MMC are sequentially defined as R, W, Z, S, U, X, T, V, Y.

To facilitate the circuit analysis of the system, the cascaded submodules in each branch can be equated with a controlled voltage source, and thus a simplified circuit model of the nonagonal MMC is shown in Fig. 2. The branches of nonagonal MMC are named as Branch-x, where x=1,2,3,4,5,6,7,8,9. Define the branch voltage as u_x, the branch current as i_x, and the circulating current as i_{cir}. The neutral points of the source/load connected with the ports are respectively O, N1, and N2. Note that u_{N1} represents the offset voltage from N1 to O; u_{N2} represents the offset voltage from N2 to O. The reference direction of each electrical quantity is shown in Fig. 2.

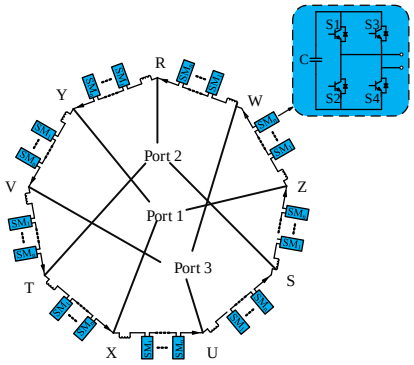

Figure 1 Nonagonal MMC topology.

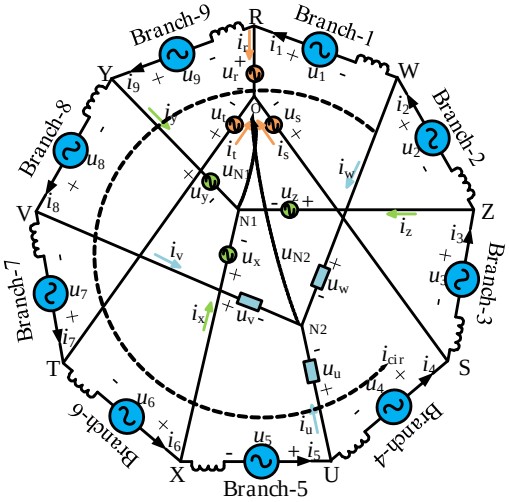

Figure 2 Simplified circuit model of nonagonal MMC.

2.2 | Mathematical model

Before the port reduction control can be introduced, the mathematical model of nonagonal MMC should first be derived. The expressions of the branch voltages can be easily obtained by Kirchhoff's voltage law:

$$\begin{cases} u_1 = u_r - u_w - u_{N2} & u_2 = u_w - u_z - u_{N1} + u_{N2} & u_3 = u_z - u_s + u_{N1} \\ u_4 = u_s - u_u - u_{N2} & u_5 = u_u - u_x - u_{N1} + u_{N2} & u_6 = u_x - u_t + u_{N1} \\ u_7 = u_t - u_v - u_{N2} & u_8 = u_v - u_y - u_{N1} + u_{N2} & u_9 = u_y - u_r + u_{N1} \end{cases} \tag{1}$$

The expressions of the branch currents, however, are a little less apparent. To obtain their expressions, an equivalent model is given in Fig. 3.

From the point of each port, the converter can be seen as a delta converter. Hence, the port is changed to delta connection as shown in the figure, and the line currents of each port are given instead of phase currents. In this way, the expressions of the branch currents of nonagonal MMC can be derived:

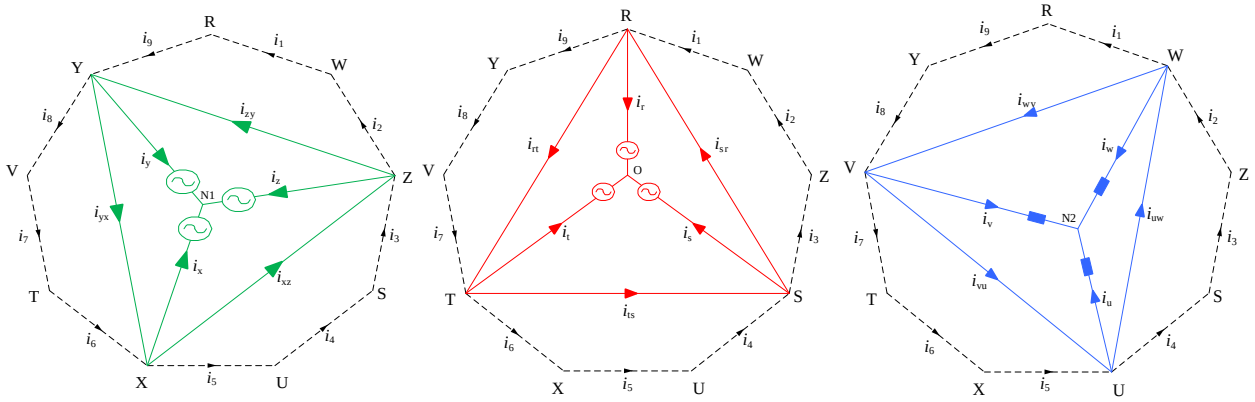

Figure 3 Equivalent diagram of the three ports.

$$\begin{cases} i_1 = i_{zy} + i_{sr} + i_{wv} + i_{cir} & i_2 = i_{zy} + i_{sr} + i_{uw} + i_{cir} \\ i_3 = i_{xz} + i_{sr} + i_{uw} + i_{cir} & i_4 = i_{xz} + i_{ts} + i_{uw} + i_{cir} \\ i_5 = i_{xz} + i_{ts} + i_{vu} + i_{cir} & i_6 = i_{yx} + i_{ts} + i_{vu} + i_{cir} \\ i_7 = i_{yx} + i_{rt} + i_{vu} + i_{cir} & i_8 = i_{yx} + i_{rt} + i_{wv} + i_{cir} \\ i_9 = i_{zy} + i_{rt} + i_{wv} + i_{cir} \end{cases} \tag{2}$$

where i_{zy}, i_{xy}, i_{yx}, i_{sr}, i_{ts}, i_{rt}, i_{wv}, i_{uw}, and i_{vu} are line currents of the equivalent triangular power supply.

Adding together the equations in (2), with port currents cancelled out, the expression of the circulating current i_{cir} can be gotten:

$$i_{cir} = (i_1 + i_2 + i_3 + i_4 + i_5 + i_6 + i_7 + i_8 + i_9)/9 \tag{3}$$

The three-phase voltage and current signals of the three ports are defined as:

$$\begin{cases} u_x = \sqrt{2}U_1 \sin\omega_1 t & i_x = \sqrt{2}I_1 \sin(\omega_1 t - \varphi_1) \\ u_r = \sqrt{2}U_2 \sin(\omega_2 t - \psi_1) & i_r = \sqrt{2}I_2 \sin(\omega_2 t - \psi_1 - \varphi_2) \\ u_u = \sqrt{2}U_3 \sin(\omega_3 t - \psi_2) & i_u = \sqrt{2}I_3 \sin(\omega_3 t - \psi_2 - \varphi_3) \end{cases} \tag{4}$$

where φ_1, φ_2, φ_3 respectively represent the phase differences between the voltage and current of the three ports; ψ_1 represents the voltage phase difference between port 2 and port 1; ψ_2 represents the voltage phase difference between port 3 and port 1. Note that phase voltages and currents of y and z lag behind phase x $2\pi/3$ and $4\pi/3$ respectively; phase voltages and currents of s and t lag behind phase r $2\pi/3$ and $4\pi/3$ respectively; phase voltages and currents of v and w lag behind phase u $2\pi/3$ and $4\pi/3$ respectively.

Taking Branch-1 for example, there are four current components flowing through it: i_{zy}, i_{sr}, i_{wv} and i_{cir}. The mathematical expressions of current i_{zy}, i_{sr} and i_{wv} can be derived by (4):

$$\begin{cases} i_{zy} = \dfrac{\sqrt{2}}{\sqrt{3}} I_1 \sin(\omega_1 t - \varphi_1 - \dfrac{3\pi}{6}) \\ i_{sr} = \dfrac{\sqrt{2}}{\sqrt{3}} I_2 \sin(\omega_2 t - \psi_1 - \varphi_2 + \dfrac{\pi}{6}) \\ i_{wv} = \dfrac{\sqrt{2}}{\sqrt{3}} I_3 \sin(\omega_3 t - \psi_2 - \varphi_3 + \dfrac{3\pi}{6}) \end{cases} \tag{5}$$

Knowing this, the voltage and current expressions of Branch-1 can be obtained as follows:

$$\begin{cases} u_1 = \sqrt{2}U_2 \sin(\omega_2 t - \psi_1) \\ -\sqrt{2}U_3 \sin(\omega_3 t - \psi_2 - \dfrac{4\pi}{3}) - u_{\mathrm{N}2} \\ i_1 = \dfrac{\sqrt{2}}{\sqrt{3}} I_1 \sin(\omega_1 t - \varphi_1 - \dfrac{3\pi}{6}) \\ + \dfrac{\sqrt{2}}{\sqrt{3}} I_2 \sin(\omega_2 t - \psi_1 - \varphi_2 + \dfrac{\pi}{6}) \\ + \dfrac{\sqrt{2}}{\sqrt{3}} I_3 \sin(\omega_3 t - \psi_2 - \varphi_3 + \dfrac{3\pi}{6}) + i_{\mathrm{cir}} \end{cases} \tag{6}$$

Similarly, the voltage and current expressions of the other branches of nonagonal MMC can also be obtained.

2.3 | Power analysis

To ensure the stable operation of nonagonal MMC, it is necessary to study the power flow of the converter, analyze its power distribution, and obtain the power balance condition.

From Fig. 2, the instantaneous power of each branch can be derived as:

$$p_j = u_j \cdot i_j \tag{7}$$

where subscript *j* represents the serial number of the converter branch.

The power expression of Branch-1 is given in Appendix. There are 13 frequency components, and the power expression of the other branches are similar. Therefore, the average power of the converter branch in a cycle is derived as follows:

$$P_j = \frac{1}{T}\int_{t-T}^{t} p_j dt = \frac{1}{T}\int_{t-T}^{t} \begin{pmatrix} p_j^{\mathrm{const}} + p_j^{\omega_1} + p_j^{\omega_2} + p_j^{\omega_3} + p_j^{2\omega_1} + p_j^{2\omega_2} \\ + p_j^{2\omega_3} + p_j^{\omega_1-\omega_2} + p_j^{\omega_2-\omega_3} + p_j^{\omega_3-\omega_1} + p_j^{\omega_1+\omega_2} \\ + p_j^{\omega_2+\omega_3} + p_j^{\omega_3+\omega_1} \end{pmatrix} dt \tag{8}$$

where P_j^{const} is the constant power component of each branch and other terms are periodic components.

It can be seen that P_j^{const} becomes an aperiodic component after integration, causing energy accumulation on the branch over time. It will affect the DC voltage stability of the converter, endangering its stable operation. As for the other frequency components, they are still periodic components after integration, hence the DC voltage fluctuation caused by them will not cause energy accumulation. In summary, the constant power component is the main factor affecting converter power balance. In order to ensure stable operation of the converter, the following conditions must be met:

$$P_j^{\mathrm{const}} = 0 \tag{9}$$

From (9) and Appendix, taking Branch-1, Branch-2, and Branch-3 of nonagonal MMC for example, the expressions of the branch constant power components are:

$$\begin{cases} P_{\text{Branch-1}}^{\mathrm{const}} = \dfrac{1}{\sqrt{3}} U_2 I_2 \cos(\varphi_2 - \dfrac{\pi}{6}) - \dfrac{1}{\sqrt{3}} U_3 I_3 \cos(\varphi_3 + \dfrac{\pi}{6}) - u_{\mathrm{N}2} i_{\mathrm{cir}} \\ P_{\text{Branch-2}}^{\mathrm{const}} = -\dfrac{1}{\sqrt{3}} U_1 I_1 \cos(\varphi_1 + \dfrac{\pi}{6}) + \dfrac{1}{\sqrt{3}} U_3 I_3 \cos(\varphi_3 - \dfrac{\pi}{6}) + (u_{\mathrm{N}2} - u_{\mathrm{N}1}) i_{\mathrm{cir}} \\ P_{\text{Branch-3}}^{\mathrm{const}} = \dfrac{1}{\sqrt{3}} U_1 I_1 \cos(\varphi_1 - \dfrac{\pi}{6}) - \dfrac{1}{\sqrt{3}} U_2 I_2 \cos(\varphi_2 + \dfrac{\pi}{6}) + u_{\mathrm{N}1} i_{\mathrm{cir}} \end{cases} \tag{10}$$

Adding the three equations in (10) together, there is:

$$P_{\text{Branch-1}}^{\mathrm{const}} + P_{\text{Branch-2}}^{\mathrm{const}} + P_{\text{Branch-3}}^{\mathrm{const}} = U_1 I_1 \cos\varphi_1 + U_2 I_2 \cos\varphi_2 + U_3 I_3 \cos\varphi_3 \tag{11}$$

The active and reactive power of the three ports of nonagonal MMC are given:

$$\begin{cases} p_{\mathrm{P1}} = 3U_1 I_1 \cos\varphi_1 \\ p_{\mathrm{P2}} = 3U_2 I_2 \cos\varphi_2 \\ p_{\mathrm{P3}} = 3U_3 I_3 \cos\varphi_3 \\ q_{\mathrm{P1}} = 3U_1 I_1 \sin\varphi_1 \\ q_{\mathrm{P2}} = 3U_2 I_2 \sin\varphi_2 \\ q_{\mathrm{P3}} = 3U_3 I_3 \sin\varphi_3 \end{cases} \tag{12}$$

where the subscripts P1, P2, and P3 respectively represent port 1, port 2, and port 3 of nonagonal MMC.

Combining (9)-(12), it can be obtained that:

$$\begin{cases} p_{\mathrm{P1}} + p_{\mathrm{P2}} + p_{\mathrm{P3}} = 0 \\ i_{\mathrm{cir}} u_{\mathrm{N1}} = -\dfrac{1}{6}(p_{\mathrm{P1}} - p_{\mathrm{P2}}) - \dfrac{\sqrt{3}}{18}(q_{\mathrm{P1}} + q_{\mathrm{P2}}) \\ i_{\mathrm{cir}} u_{\mathrm{N2}} = \dfrac{1}{6}(p_{\mathrm{P2}} - p_{\mathrm{P3}}) + \dfrac{\sqrt{3}}{18}(q_{\mathrm{P2}} + q_{\mathrm{P3}}) \end{cases} \tag{13}$$

From (13), the first term represents the port power balance condition of the nonagonal MMC. To ensure that the input power equals the output power, the first term has to be sufficed. The second term and the third term represent the power balance condition within nonagonal MMC. It can be seen that offset voltages should be injected to eliminate the power imbalance between different branches.

3 | NONAGONAL MMC PORT REDUCTION OPERATION

When an AC port of the nonagonal MMC needs to be exited for maintenance, the port should be turned off and isolated so as to ensure the normal operation of other systems. During port disconnection, the nonagonal MMC should continue to operate under a dual port condition, which necessitate the proposal of a port reduction control to ensure the stable operation during this phase. The main idea of the port reduction control proposed in this paper is to switch the nonagonal MMC to a hexagonal MMC which is an AC-AC topology of a similar circular structure but has only two ports.

In this section, the structure of the hexagonal MMC and its power balance condition are first given for the benefit of the introduction of nonagonal MMC port reduction control. Then, the nonagonal MMC port reduction topology is presented, and its working principles are then analyzed.

3.1 | Hexagonal MMC

The structure of the hexagonal MMC and its power balance condition are also given in this section for the benefit of the introduction of nonagonal MMC port reduction control. Fig. 4 shows the basic configuration of hexagonal MMC, which can connect two three-phase systems of different frequencies. The topology comprises six modular multilevel branches. Each branch consists of cascaded H-bridge submodules and a series inductor. As each branch connected one phase of port 1 to one phase of port 2, the branch voltage contains both phase voltages. Take Branch-1 for example, its branch voltage can be derived as:

$$u_1 = u_{\mathrm{r}} - u_{\mathrm{z}} - u_{\mathrm{N1}} \tag{14}$$

Similarly, to ensure stable operation, the DC-link capacitor of each submodule should be of a steady value. Therefore, the constant component of hexagonal MMC branch power needs to satisfy (9). According to [25], it can be obtained:

$$i_{\mathrm{cir}} u_{\mathrm{N1}} = -(-1)^n \frac{1}{6}(p_{\mathrm{P1}} + p_{\mathrm{P2}}) - \frac{\sqrt{3}}{18}(q_{\mathrm{P1}} - q_{\mathrm{P2}}) \tag{15}$$

Equation (15) is the power balance condition for hexagonal MMC, i_{cir} and u_{N1} is injected to achieve power balance.

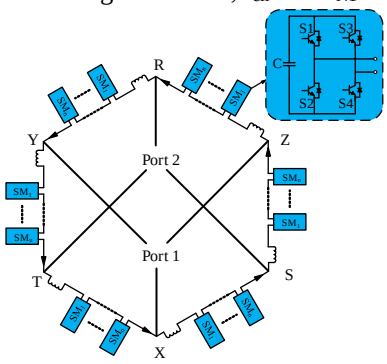

Figure 4 Hexagonal MMC topology.

3.2 | Port reduction topology

When one port is disconnected, the nonagonal MMC is shown in Fig. 5. It should be noted that as the main purpose of nonagonal MMC is frequency conversion instead of voltage boost or reduction, the voltage ratio of the three ports is usually set as 1:1:1 with transformers connected outside for voltage boost or reduction [27]. Hence, it is supposed in this paper that all nine branches of the nonagonal MMC have n numbers of submodules.

After port reduction, to ensure the continual stable operation of the converter, the nonagonal MMC control strategy is optimized. The optimized control strategy needs to make sure that the number of submodules put into use in branch-1,3,5 are the same as that in branch-2,4,6. In this way, the nonagonal MMC minus one port can smoothly switch to a quasi-hexagonal MMC operation. To achieve this, the obvious way is to turn off three branches so that there are only six branches in operation. Considering the circular structure, the open circuit of one branch will cause the shutoff of the whole converter. Hence, the three branches should be bypassed. However, this would leave the submodule capacitors floating in the said branches, and may cause power fluctuations when nonagonal MMC switches back to its normal three port operation. To avoid this, the submodules in branches connected with the offline port are operated alternately.

As shown in Fig. 5, by rearranging nine branches into six branches, the nonagonal MMC can be seen as a quasi-hexagonal MMC. The branches of the port reduction topology are named as branch-1,2,3,4,5,6. For branch-1,3,5, each branch consists of 2n cascaded submodules and two series inductors. For branch-2,4,6, each branch consists of n cascaded submodules with one series inductor. Divide the branches of the port reduction topology into three groups: branch-1 and branch-2; branch-3 and branch-4; branch-5 and branch-6. Take Group 1 (branch-1,2) for example, branch-1 and branch-2 of the port reduction topology correspond to the Branch-1, Branch-2, and Branch-3 of the nonagonal MMC. In this case, define the submodule numbers on Branch-1,2,3 as Bij (i=1,2,3; j=1,2,3,4), the operating state of the port reduction topology in a switching cycle is shown in Table I. Suppose that each branch has four submodules, and the inductors on each branch are of the same value.

According to the operation modes of Table I, two modes is shown in Fig. 6. Mode 1 is shown in Fig. 6 (a), when the converter works in mode 1, B11, B12, B21 and B22 will be put into operation and all submodules on branch-2 will also be put into operation. By controlling the state of IGBT, the submodule port output voltage can be switched to 0 V, $+U_{dc}$, or $-U_{dc}$. By overlaying the output voltage of submodule, multilevel waveforms are generated. At the same time, B13, B14, B23, and B24 are in the bypass state, and the output voltage is 0 V, the capacitor voltage of submodule DC side will not be charged and discharged, thus, it does not affect the stable operation of the converter.

Mode 2 is shown in Fig. 6 (b), when the converter works in mode 2, in this case, B11, B12, B21 and B22 will be bypassed, while B13, B14, B23 and B24 is put into operation. All submodules on branch-2 are also put into operation. The same analysis can be applied to the other groups. In this way, the converter can achieve stable operation.

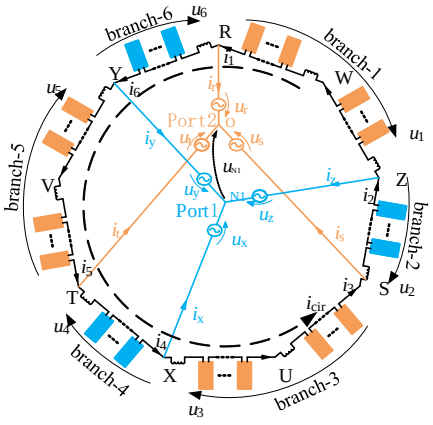

Figure 5 Port reduction topology.

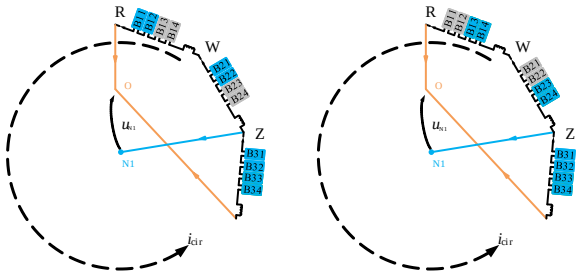

(a) model 1 (b) model 2

Figure 6 Operation models of port reduction topology.

Table 1 Port reduction topology branch-1 and branch-2 operating state table

H-bridge submodule	B11	B12	B13	B14	B21	B22	B23	B24	B31	B32	B33	B34
Model 1 (0≤t≤ Ts/2)	Put In	Put In	Bypass	Bypass	Put In	Put In	Bypass	Bypass	Put In	Put In	Put In	Put In
Model 2 (Ts/2≤t≤ Ts)	Bypass	Bypass	Put In	Put In	Bypass	Bypass	Put In	Put In	Put In	Put In	Put In	Put In

4 | SYSTEM CONTROL STRATEGY

4.1 | Case study

In the article, the converter is applied to distributed generation (DG) and local consumption applications. Port 3, i.e, local load, is taken as the offline port for example. When all three ports are turned on, the DG will not only power the local loads, but also feed the additional power to the grid. When one of the ports need to disconnect from the other two systems, the DG generated power is transmitted wholly to the grid. Fig. 7 presents the relationship between the energy interaction of the circular MMC ports.

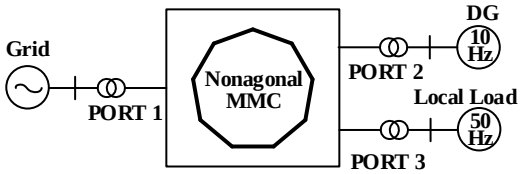

(a) Nonagonal MMC operation

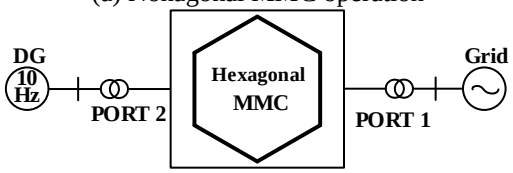

(b) Hexagonal MMC operation

Figure 7 Energy interaction under different scenarios (a) Nonagonal MMC operation; (b) Hexagonal MMC operation.

4.2 | Proposed reduced port control strategy

To ensure the stable operation of nonagonal MMC after reducing one port, the article proposes an overall port reduction operation strategy, as shown in Fig. 8. When a port needs to be isolated, define its state as 1, as shown in Fig. 8. When the state of all three ports remains 0, the nonagonal MMC continue to operate under nonagonal MMC control. The detailed control strategy of the nonagonal MMC has been introduced in [26]. When port disconnection is required, the nonagonal MMC port reduction operation control strategy is used, and the corresponding control strategy is shown in Fig. 9. The control strategy consists of DC-link voltage control, branch power balance control, alternate operation control of branch submodules, and DC-link voltage regulation in branch.

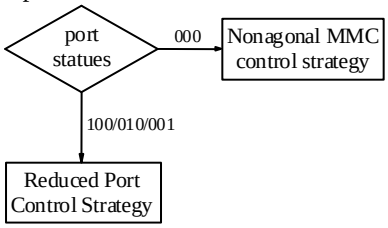

Figure 8 Overall port reduction operation strategy

1) DC-link voltage control: Port 1 is connected with AC grid and adopts DC-link voltage control to ensure that the input power equals the output power so that energy will not accumulate in the converter, hence the voltage on the DC-link capacitor will not collapse.

2) Branch power balance control: It focuses on the submodule capacitor voltage difference between different branches, which is caused by the constant component of branch power. To address this issue, the average values of submodule capacitor voltages of different branches are obtained: $U_{dc\_1\_avg}$, $U_{dc\_2\_avg}$, $U_{dc\_3\_avg}$, $U_{dc\_4\_avg}$, $U_{dc\_5\_avg}$, $U_{dc\_6\_avg}$. $U_{dc\_i\_avg}$ depicts the average submodules capacitor voltage of all the submodules in branch i, in which i=1,2,3,4,5,6; U_{dc_135} depicts the average value of the submodule capacitor voltage of all the submodules in branch 1,3,5; U_{dc_246} depicts the average value of the submodule capacitor voltage of all the submodules in branch 2,4,6. The offset voltage U_{N1} and ($-U_{N1}$) are obtained by choosing maximum deviation value, and the instruction are required to closely follow the working state of the system. Branch power balance is achieved by superimposing offset voltages over the voltage modulation waves.

3) DC-link voltage regulation in branch: The DC-link voltage balance of the submodules within one branch is achieved by the DC-link voltage regulation in branch. By detecting the capacitor voltage of each submodule within one branch and compares it with the average value, the control adjusts the modulation wave, and then this indirectly adjusts the charging and discharging time of the capacitor to achieve voltage equalization. U_{dc_ji} (i=1,…, n) depicts the capacitor voltage of the i-th submodule in branch j.

4) Alternate operation control of branch submodules: During a port disconnection, the nonagonal MMC should continue to operate under a dual port condition, which necessitate the proposal of a port reduction control to ensure the stable operation during this phase. The principle of the control strategy designed in this part is as follows. For the submodules that need to be invested in the branch, the pulse signal output by CPS-SPWM is distributed, and it runs alternately every half of the switching cycle. The alternating period as follows:

$$T_s \cdot (n-1) \le t \le \frac{T_s}{2} + T_s \cdot (n-1) \tag{16}$$

$$\frac{T_s}{2} + T_s \cdot (n-1) \le t \le T_s + T_s \cdot (n-1) \tag{17}$$

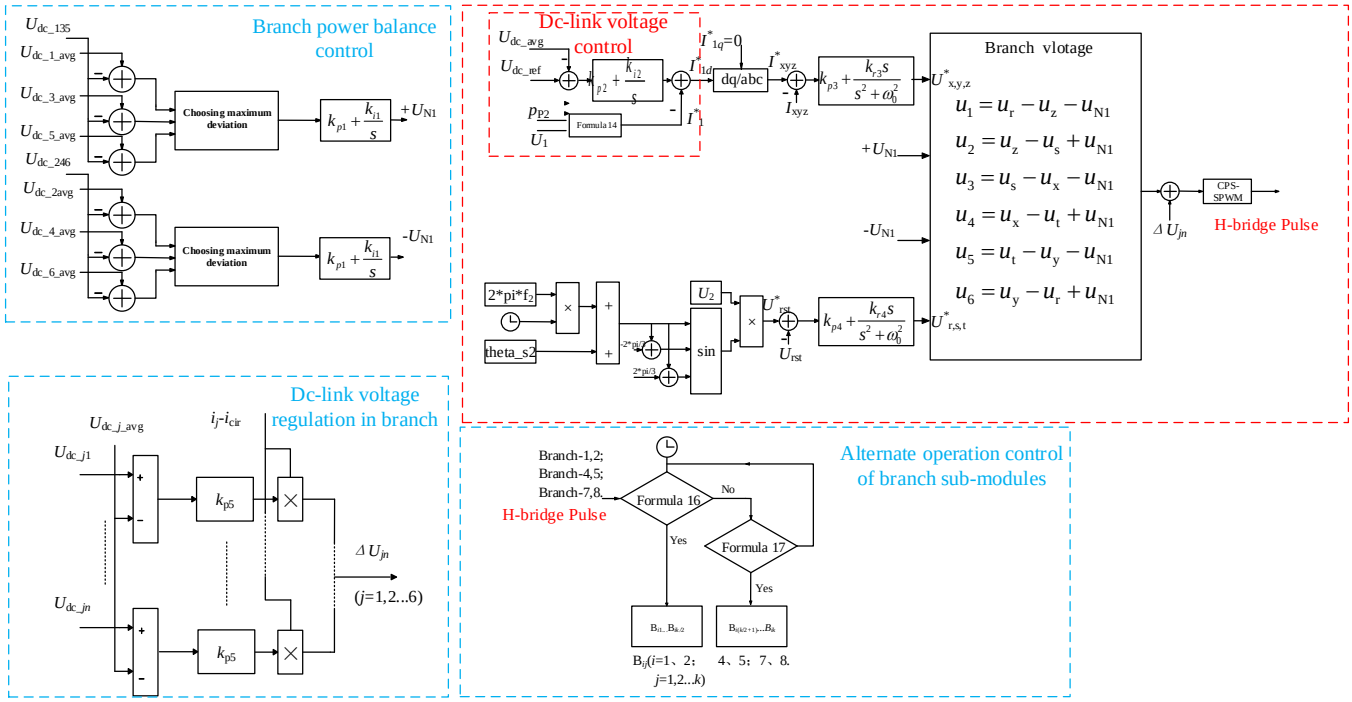

Figure 9 Nonagonal MMC port reduction operation control strategy

5 | RTLAB SIMULATION VERIFICATION

The effectiveness of the control strategy is verified through RTLAB. The system parameters and converter parameters are given in Tables II and III.

In this simulation, the line voltage and frequency of port 1 and port 2 are all 6 kV and 50 Hz. Then, the port 3 frequency is 10 Hz so as to test the low frequency performance of the nonagonal MMC.

Table 2 System parameters

Parameter	Value
Port 1: Rated line voltage/kV	6
Port 1: Rated frequency/Hz	50
Port 1: Filter inductance/mH	5
Port 2: Rated line voltage/kV	6
Port 2: Rated phase current/A	200
Port 2: Rated frequency/Hz	50
Port 3: Rated line voltage /kV	6
Port 3: Rated phase current /A	110-150
Port 3: Rated frequency /Hz	10
Port 3: Resistance/Ω	22.5
Port 3: Inductance/mH	5

Table 3 Converter parameters

Parameters	Value	Parameters	Value
k_{p1}	0.0001	k_{i1}	0.04
k_{p2}	0.5	k_{i2}	10
k_{p3}	0.006	k_{r3}	0.06
k_{p4}	0.0005	k_{r4}	0.05
k_{p5}	0.2	Number of submodules	4
DC-link capacitance/mF	10	DC-link voltage/V	3535
Switching frequency of H-bridge/Hz	1000	Branch inductance/mH	0.25

The waveforms of port power are given in Fig. 10. It can be seen that before 1 s, the power of port 2 is 2.08 MW and the power generated is enough to power port 3. At 1.0 s, port 3 is disconnected so that the control of nonagonal MMC is switched to port reduction control. At 1.2 s, the power generated by port 2 is decreased from 2.08 MW to 1.38 MW to test the dynamic performance of the port reduction control.

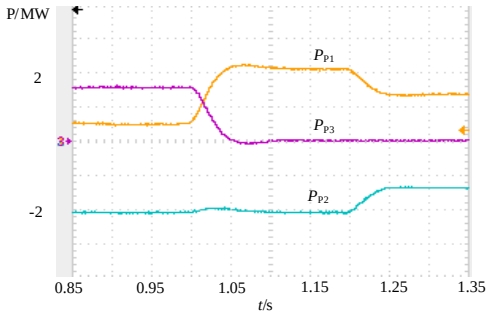

Figure 10 Port power waveform.

As seen from Fig. 11 and Fig. 12, at 1.0 s, the nonagonal MMC can switch smoothly from three ports to two ports with no noticable overshoots in both port voltages and port currents. The amplitudes of the port voltages of the remaining ports does not change, while the RMS of the phase current of port 1 is increased from 48.3 A to 200.2 A due to the disconnect of port 3.

At 1.2 s, when the phase current of port 2 is decreased from 200.0 A to 133.4 A, the current of Port 1 follows the change smoothly indicating that the port reduction control has good dynamic performance. The amplitudes of the port voltages of the remaining ports does not change, while the RMS of the phase current of port 1 decreases to 132.8 A after 1.2 s, which is caused by the decrease of power of port 2.

The average DC-link voltages of Branch 1,2,3 are given in Fig. 13. It can be seen that during the whole process, the DC-link voltages of the submodules on different branches approximately stable at 3535 V, indicating that the nonagonal MMC can still keep its power balance under port reduction condition.

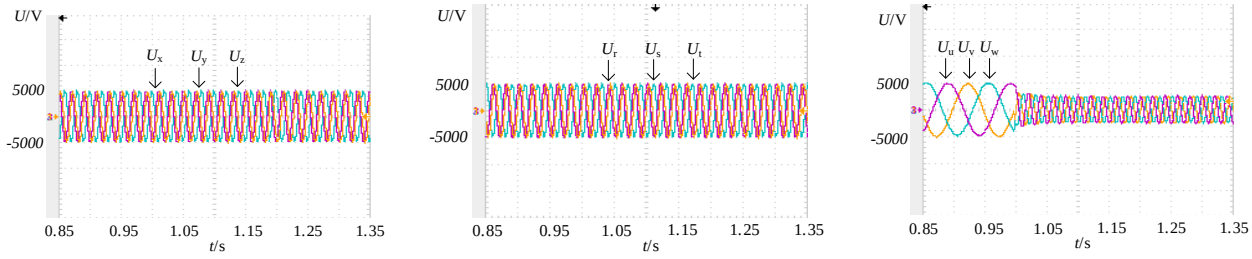

(a) port 1 voltage waveform (b) port 2 voltage waveform (c) port 3 voltage waveform

Figure 11 Port voltage waveform.

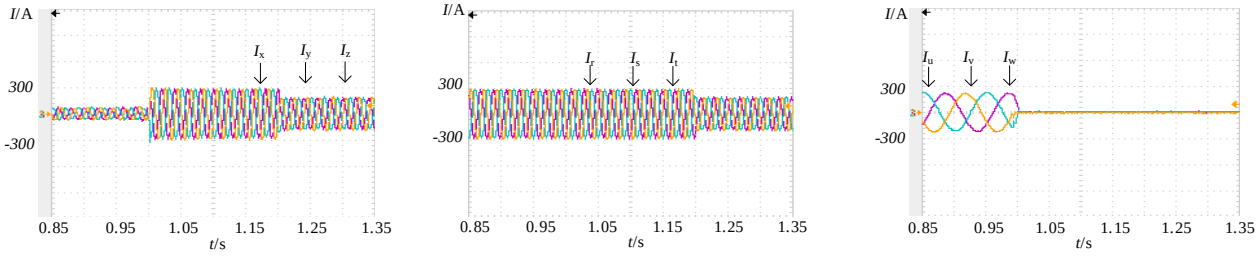

(a) Port 1 current waveform (b) Port 2 current waveform (c) Port 3 current waveform

Figure 12 Port current waveform.

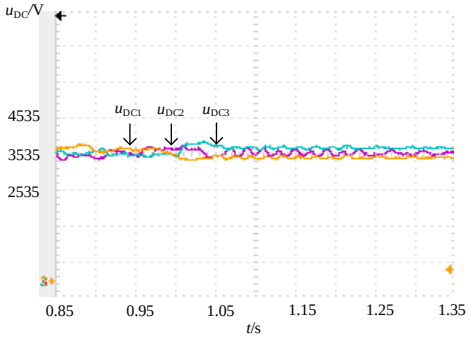

Figure 13 DC-link voltage waveform.

6 | CONCLUSION

A control scheme for nonagonal MMC port reduction operation is proposed in this paper. By rearranging the submodules, it allows the nonagonal MMC to operate as a quasi-hexagonal MMC ensuring the safe operation of the remaining ports when one of the ports is disconnected. By alternately operating the submodules, no submodule capacitors are left floating, avoiding disruptions and large capacitor voltage fluctuations. The proposal of the control improves the practical value of nonagonal MMC and enables it to operate as an SOP. It also helps to unite the nonagonal MMC and hexagonal MMC as one circular MMC, allowing it to switch fluently between two port operation and three port operation.

References

1. F. Sun, X. Li, X. Du and L. Chen, "Long-Term Planning of Shared Energy Storage for Multiple Renewable Energy Bases Considering the Growth of Renewables and Load Demand," 2022 4th International Conference on Power and Energy Technology (ICPET), Beijing, China, October. 2022, pp. 800-805.
2. X. Ge, J. Qian, Y. Fu, W. -J. Lee and Y. Mi, "Transient Stability Evaluation Criterion of Multi-Wind Farms Integrated Power System," in IEEE Transactions on Power Systems, vol. 37, no. 4, pp. 3137-3140, July 2022.
3. A. Zafari, M. Mehrasa, S. Bacha, K. Al-Haddad and N. Hosseinzadeh, "A Robust Fractional-Order Control Technique for Stable Performance of Multilevel Converter-Based Grid-Tied DG Units," in IEEE Transactions on Industrial Electronics, vol. 69, no. 10, pp. 10192-10201, Oct. 2022.
4. X. Jiang, Y. Zhou, W. Ming, P. Yang and J. Wu, "An Overview of Soft Open Points in Electricity Distribution Networks," in IEEE Transactions on Smart Grid, vol. 13, no. 3, pp. 1899-1910, May 2022.
5. J. Fang, S. Yang, H. Wang, and N. Tashakor a, “Reduction of MMC Capacitances Through Parallelization of Symmetrical Half-Bridge Submodules,” *IEEE Trans. Power Electron*., vol. 36, no. 8, pp. 8907-8918, Aug. 2021.
6. W. Wang, K. Ma and X. Cai, “Efficient Capacitor Voltage Balancing Method for Modular Multilevel Converter Under Carrier-Phase-Shift Pulsewidth Modulation,” *IEEE Trans. Power Electron*., vol. 36, no. 2, pp. 1553-1562, Feb. 2021.
7. A. Lewicki, C. Odeh and M. Morawiec, "Space Vector Pulsewidth Modulation Strategy for Multilevel Cascaded H-Bridge Inverter With DC-Link Voltage Balancing Ability," in IEEE Transactions on Industrial Electronics, vol. 70, no. 2, pp. 1161-1170, Feb. 2023.

8. L. Zhang, W. Hong, C. Gao, R. Liu, Q. Yu and C. Wei, "Selected Harmonic Mitigation PWM Power Matching Control Strategy for Asymmetric Cascaded H-Bridge Multilevel Inverter," in IEEE Journal of Emerging and Selected Topics in Power Electronics, vol. 10, no. 4, pp. 4059-4072, Aug. 2022.
9. R. kumar, P. Kant and B. Singh, "Harmonic Suppression Scheme for Multi-Pulse Converter Fed Multilevel Inverter Based IM Drive," in *Proc PIICON*, Sonepat, India, 2020, pp. 1-6.
10. R. Kumar, P. Kant and B. Singh, "Modified PWM Technique for a Multi-Pulse Converter fed Multilevel Inverter Based IM Drive," in *Proc. PESGRE*, Cochin, India, 2020, pp. 1-6.
11. C. Zhao, Q. Fan, S. Li and J. Xu, "Operation Method of MMC Capacitance Reduction Under Arm Inductor Switching Control," *IEEE Trans. Power Del*., vol. 36, no. 1, pp. 418-428, Feb. 2021.
12. C. Enang and B. K. Johnson, "Enhanced Modular Multilevel Converter Based STATCOM with Hybrid Energy Storage," in *Proc. PESGM*, Atlanta, GA, USA, 2019, pp. 1-5.
13. A. Elserougi, I. Abdelsalam, A. Massoud and S. Ahmed, "Modular Multilevel Converter With Self-Energy Equalization for Medium Voltage AC Drive Applications," *IEEE Trans. Ind. Electron*., vol. 68, no. 12, pp. 11881-11894, Dec. 2021.
14. Y. S. Kumar and G. Poddar, "Balanced Submodule Operation of Modular Multilevel Converter-Based Induction Motor Drive for Wide-Speed Range," *IEEE Trans. Power Electron*., vol. 35, no. 4, pp. 3918-3927, April 2020.
15. B. Li, J. Hu, S. Zhou and D. Xu, "Hybrid back-to-back MMC system for variable speed AC machine drives," *CPSS Trans. Power Electron. and Appl.*, vol. 5, no. 2, pp. 114-125, June 2020.
16. F. Rong, S. Xu, L. Pan and Z. Sun, "Transformerless Grid Connected Control of Wind Turbine Based on H-MMC," in IEEE Journal of Emerging and Selected Topics in Power Electronics, vol. 10, no. 2, pp. 2126-2137, April 2022.
17. S. Liu, B. Zhao, Y. Chen, G. Wang and X. Wang, "Optimal Arm Current Reallocation of Modular Multilevel Matrix Converter Dedicated for Power Grid Interconnection," in IEEE Transactions on Power Delivery, vol. 37, no. 5, pp. 3477-3490, Oct. 2022.
18. J. Luo, X. -P. Zhang, Y. Xue, K. Gu and F. Wu, "Harmonic Analysis of Modular Multilevel Matrix Converter for Fractional Frequency Transmission System," IEEE Trans. Power Del., vol. 35, no. 3, pp. 1209-1219, June 2020.
19. C. Wang, Z. Zheng, K. Wang, B. Yang, P. Zhou and Y. Li, "Analysis and Control of Modular Multilevel Matrix Converters Under Branch Fault Conditions," in IEEE Transactions on Power Electronics, vol. 37, no. 2, pp. 1682-1699, Feb. 2022.
20. Y. Meng, B. Liu, H. Luo, S. Shang, H. Zhang and X. Wang, "Control scheme of hexagonal modular multilevel direct converter for offshore wind power integration via fractional frequency transmission system," in Journal of Modern Power Systems and Clean Energy, vol. 6, no. 1, pp. 168-180, January 2018.
21. J. Jiang, S. Hu, S. Liu, Z. Lu, H. Huang and W. Wu, "Smooth Transition of Modular Multilevel Matrix Converter to Hexverter During Single-Arm Failure," 2022 IEEE 6th Conference on Energy Internet and Energy System Integration (EI2), Chengdu, China, 2022, pp. 50-56.
22. W. Huang, F. Liu, W. Liu, Y. Zhuang, Y. Huang and X. Zha, "Circulating Current Generating Mechanism and Suppression Control of HMMC," in IEEE Journal of Emerging and Selected Topics in Power Electronics, vol. 10, no. 6, pp. 7297-7306, Dec. 2022.
23. Y. Yi, G. Yang, C. Qian and Y. Gui, "Branch Voltage Balancing Control Strategy Based on the Transfer Power Model by Zero-Sequence Circulating Current for the Hexverter," in IEEE Access, vol. 10, pp. 44326-44336, 2022.
24. W. Liu, F. Liu, H. Gao, Y. Zhuang and X. Zha, "A Transformerless Three-Port Nonagonal MMC for the Grid Connection and Local Consumption of Distributed Generation," in *IEEE J Em Sel Top P*, vol. 7, no. 1, pp. 108-117, March 2019.
25. S. Zhou, F. Rong, W. Sun, S. Huang, Q. Wu, "AC/AC grid connection of six-phase wind power generator based on enneagon MMC converter," international Journal of Electrical Power & Energy Systems, Volume 118, 2020.
26. W. Liu, J. Yan, Y. Wang, B. Yuan, and J. Liang, "Bridge Arm Current Stress Analysis of Circular MMC," in High Voltage Engineering, early access.
27. W. Huang, X. Zha, F. Liu, W. Liu, Y. Zhuang and Y. Huang, "Power Imbalance Analysis and Neutral Offset Voltage Decoupling Control of Nonagonal MMC Applied in FFTS," in IEEE Journal of Emerging and Selected Topics in Power Electronics, vol. 10, no. 6, pp. 7285-7296, Dec. 2022.
28. D. Ma, W. Chen, L. Shu, K. Hou, R. Liu and C. Zhang, "Multiport AC-AC-DC Converter for SNOP With One Medium-Frequency Transformer," in CPSS Transactions on Power Electronics and Applications, vol. 7, no. 4, pp. 374-385, December 2022.
29. F. Qin, F. Gao, Y. Tang, T. Xu, J. Wang and D. Niu, "Configuration and Operation of Nine-Arm Modular Multilevel Converter With Improved Hybrid Submodules," in IEEE Transactions on Power Electronics, vol. 36, no. 6, pp. 6389-6403, June 2021.

Appendix

$$
\begin{aligned}
p_1 &= (u_{\mathrm{r}} - u_{\mathrm{w}} - u_{\mathrm{N2}})(i_{\mathrm{zy}} + i_{\mathrm{sr}} + i_{\mathrm{wv}} + i_{\mathrm{cir}}) = \frac{1}{\sqrt{3}}U_2 I_2 \cos(\varphi_2 - \frac{\pi}{6}) - \frac{1}{\sqrt{3}}U_3 I_3 \cos(\varphi_3 - \frac{11\pi}{6}) - u_{\mathrm{N2}} i_{\mathrm{cir}} \\
&- \frac{\sqrt{2}}{\sqrt{3}}u_{\mathrm{N2}} I_1 \sin(\omega_1 t - \varphi_1 - \frac{3\pi}{6}) - \frac{\sqrt{2}}{\sqrt{3}}u_{\mathrm{N2}} I_2 \sin(\omega_2 t - \psi_1 - \varphi_2 - \frac{\pi}{6}) + \sqrt{2}U_2 i_{\mathrm{cir}} \sin(\omega_2 t - \psi_1) \\
&- \frac{\sqrt{2}}{\sqrt{3}}u_{\mathrm{N2}} I_3 \sin(\omega_3 t - \psi_2 - \varphi_3 + \frac{\pi}{2}) - \sqrt{2}U_3 i_{\mathrm{cir}} \sin(\omega_3 t - \psi_2 - \frac{4\pi}{3}) - \frac{1}{\sqrt{3}}U_2 I_1 \cos(\omega_1 t + \omega_2 t - \psi_1 - \varphi_1 - \frac{3\pi}{6}) \\
&- \frac{1}{\sqrt{3}}U_2 I_3 \cos(\omega_2 t + \omega_3 t - \psi_1 - \psi_2 - \varphi_3 + \frac{\pi}{2}) + \frac{1}{\sqrt{3}}U_3 I_1 \cos(\omega_1 t + \omega_3 t - \psi_2 - \varphi_1 - \frac{9\pi}{6}) \\
&+ \frac{1}{\sqrt{3}}U_3 I_2 \cos(\omega_2 t + \omega_3 t - \psi_1 - \psi_2 - \varphi_2 - \frac{7\pi}{6}) + \frac{1}{\sqrt{3}}U_2 I_1 \cos(\omega_2 t - \omega_1 t - \psi_1 + \varphi_1 + \frac{3\pi}{6}) \\
&+ \frac{1}{\sqrt{3}}U_2 I_3 \cos(\omega_2 t - \omega_3 t - \psi_1 + \psi_2 + \varphi_3 - \frac{\pi}{2}) - \frac{1}{\sqrt{3}}U_3 I_1 \cos(\omega_3 t - \omega_1 t - \psi_2 + \varphi_1 - \frac{5\pi}{6}) \\
&- \frac{1}{\sqrt{3}}U_3 I_2 \cos(\omega_3 t - \omega_2 t - \psi_2 + \psi_1 + \varphi_2 - \frac{9\pi}{6}) - \frac{1}{\sqrt{3}}U_2 I_2 \cos(2\omega_2 t - 2\psi_1 - \varphi_2 + \frac{\pi}{6}) \\
&+ \frac{1}{\sqrt{3}}U_3 I_3 \cos(2\omega_3 t - 2\psi_2 - \varphi_3 - \frac{5\pi}{6}) \\
&= p_j^{\mathrm{const}} - u_{\mathrm{N2}} i_{\mathrm{cir}} + p_j^{\omega_1} + p_j^{\omega_2} + p_j^{\omega_3} + p_j^{2\omega_1} + p_j^{2\omega_2} + p_j^{2\omega_3} + p_j^{\omega_1 - \omega_2} + p_j^{\omega_2 - \omega_3} + p_j^{\omega_3 - \omega_1} + p_j^{\omega_1 + \omega_2} + p_j^{\omega_2 + \omega_3} + p_j^{\omega_3 + \omega_1}
\end{aligned}
$$